Electronic supplementary information (ESI)

Siloxane-induced robust photoactive materials with high humidity tolerance for ambient processing of organic solar cells

Haizhen Liu, Dong Yuan, Haiying Jiang, Suhan Li, Lianjie Zhang*, Junwu Chen*

Institute of Polymer Optoelectronic Materials & Devices, State Key Laboratory of Luminescent Materials & Devices, South China University of Technology, Guangzhou 510640, P. R. China.

*Corresponding author: lianjiezhang@scut.edu.cn (L. Zhang), psjwchen@scut.edu.cn (J. Chen)

Materials

Polymer donor PTQ10, PQSi705, PBZ-2Si, Si25, i-IESi-4F and FC-S1 were synthesized in our lab according to the procedures in the literatures.[1-6] Polymer donor J52 and non-fullerene acceptors Y6, Y6-BO, i-IEICO-4F were purchased from Shenzhen Yirou Photovoltaic Technology Co., Ltd.

Fabrication of the OSCs

The devices were fabricated in inverted architectures of ITO/ZnO/active layer/MoO_3/Al. The patterned ITO-coated glass substrates were cleaned by sequential sonication using detergent, acetone, deionized water, and ethanol, and dried in oven at 70 ℃ before used. ZnO layer of 30 nm was spun onto the substrate and annealed at 200 ℃ on a hot plate for 30 min in air. The active layers of PTQ10:Y6 and PQSi705:Y6 were prepared by dissolving in chloroform at room temperature with a donor:acceptor mass ratio of 1:1.2 at a total concentration of 17 mg/mL. The spin-coating of an active layer was conducted at 3000 rpm for 40 s, giving an optimal film thickness of ~110 nm. Then the active layer was dried at 110 °C for 5 min. Subsequently, for devices where the active layer needs to be processed in N_2, the ITO substrates covered with ZnO were transferred to a N_2-filled glovebox (water and oxygen content < 0.1%) and then the donor and acceptor blend solutions were spin-coated on the substrates. For the devices processed in air, the active layer was directly spin-coated on the ZnO in air. The relative humidity of 65% and 93% was adjusted by a small humidifier and detected by a hygrometer. Finally, 5 nm MoO_3 and 100 nm aluminum (Al) were sequentially deposited on top of the active

layer through a shadow mask in a vacuum chamber at a pressure of 2×10^{-4} Pa. The active layer area of the device was defined to be 0.057 cm^2.

For the extremely harsh treatments of PQSi705:Y6 and PTQ10:Y6 active layers, the PQSi705:Y6 or PTQ10:Y6 solution was spin-coated on the ZnO cathode interface, and then its surface was immersed with water for 10 min or its blend film was exposed in boiling water vapor for 10 min. After the harsh treatments, the water on the surface of the active layer was thrown off and the active layer was annealed at 110°C for 5 min, and finally the MoO_3 and Al were continuously evaporated on the active layer under the pressure of 1×10^{-5} Pa to complete the device preparation.

Active layers of PBZ-2Si:i-IEICO-4F, J52:i-IESi-4F and PBZ-2Si:i-IESi-4F were fabricated according to descriptions in a previous report.[4] Active layer Si25:Y6-BO was prepared by dissolving in 80 ℃ hot chlorobenzene with a donor:acceptor mass ratio of 1:1.2 at a total concentration of 14 mg/mL. The thickness of the Si25:Y6-BO active layer is about 300 nm.

The PQSi705:*m*-THE based devices were fabricated in a conventional device structure of ITO/PEDOT:PSS/PQSi705:*m*-THE/PDINN/Ag. The optimized OSCs with D/A mass ratio of 1:1.2 at a total concentration of 17 mg/mL in chloroform, 0.7% 1-CN as solvent additive. The spin-coating of an active layer was conducted at 3000 rpm for 40 s, giving an optimal film thickness of ~100 nm, and thermal annealing at 90 ℃ for 5 min. The PDINN methanol solution with a concentration of 1.0 mg/mL was deposited on the active layer at a speed of 3000 rpm for 30 s. Under the pressure of 1×10^{-5} Pa, about 100 nm of Ag electrode was evaporated and deposited.

Measurements and characterizations

Photovoltaic performance measurements. The photovoltaic performance was measured under an AM 1.5G (air mass 1.5 global) spectrum from a solar simulator (Japan, SAN-EI, XES-40S1). The light intensity of the solar simulator was calibrated with standard silicon solar cell with a KG5 filter at 100 mW/cm^2 before the testing, as calibrated by a National Renewable Energy Laboratory (NREL) certified silicon photodiode. The current density-voltage (*J-V*) curves were recorded with a Keithley 2400 source meter.

Fourier-transform infra-red (FTIR) measurements. The FTIR absorption spectra were performed on Infrared Spectrum Microscope (Nicolet IS50 - Nicolet Continuum, Thermo Fisher Scientific Co.). The measurement was based on a reflection mode.

Absorption spectra measurements. UV-vis absorption spectra were carried out via UV-3600 (Shimadzu Co.) spectrophotometer.

EQE measurements. The external quantum efficiency (EQE) data were gained through the solar-cell spectral-response measurement system (QE-R3011, Enlitech), which was calibrated with a crystal silicon photovoltaic cell before testing.

SCLC measurements. The hole mobilities (μ_h) and electron mobilities (μ_e) of active layers were measured by the space charge limited current (SCLC) method with hole-only devices of ITO/PEDOT:PSS/Active layer/MoO_3/Al and electron-only devices of ITO/ZnO/Active layer/PFN-Br/Al. The μ_h and μ_e were determined by fitting the dark current to the model of a single carrier SCLC, described by the equation:

$$J = \frac{9}{8}\varepsilon_0\varepsilon_r\mu\frac{V^2}{d^3}$$

where J is the current, ε_0 is the permittivity of free space, ε_r is the material relative permittivity, V is the effective voltage and d is the thickness of the active layer. The effective voltage can be obtained by subtracting the built-in voltage (V_{bi}) from the applied voltage (V_{appl}), $V=V_{appl}-V_{bi}$. The mobility can be calculated from the slope of the $J^{1/2}$ -V curves.

AFM measurements. The surface morphologies of AFM images relative to the corresponding BHJ blends were obtained on a Multimode 8 Dimension Icon Scanning Probe Microscope (Bruker, Multimode 8) in the tapping mode.

TEM measurements. TEM micrographs were obtained on a JEM 1400 Plus microscope operating at 300kV.

Supplementary Figures

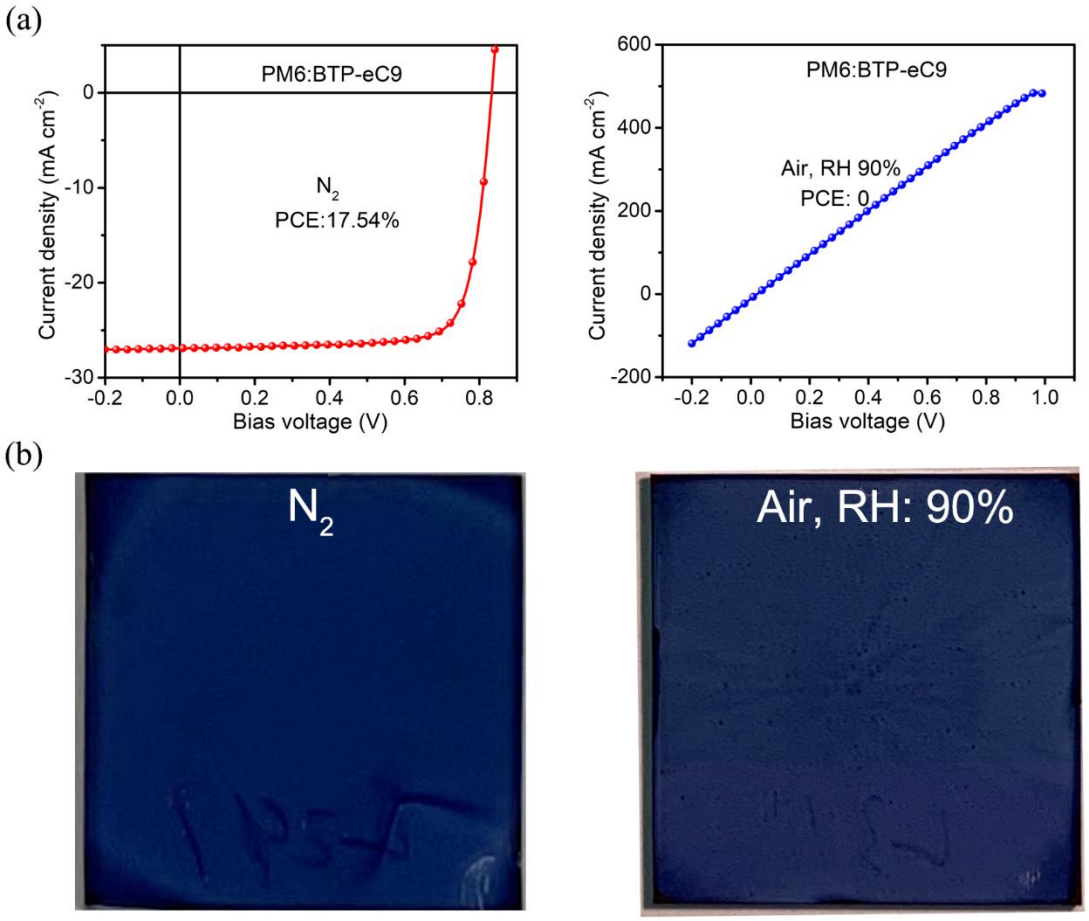

Fig. S1 (a) *J-V* curves and (b) photographs for PM6:BTP-eC9 active layers (~110 nm thickness) casted in N_2 glovebox (left) and air with 90% relative humidity (right).

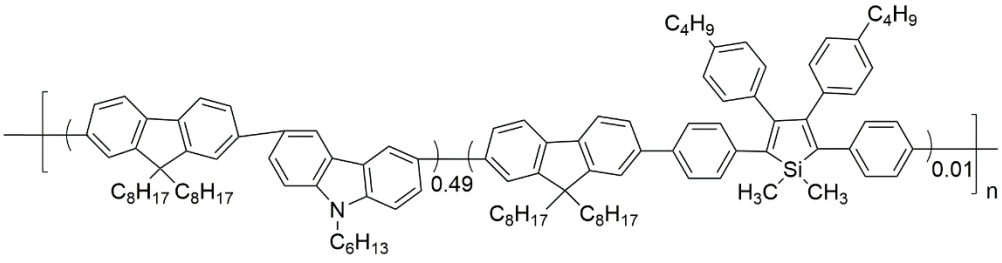

FC-S1

Fig. S2 The molecular structure of polymer FC-S1, whose synthesis was given in a previous report.[6]

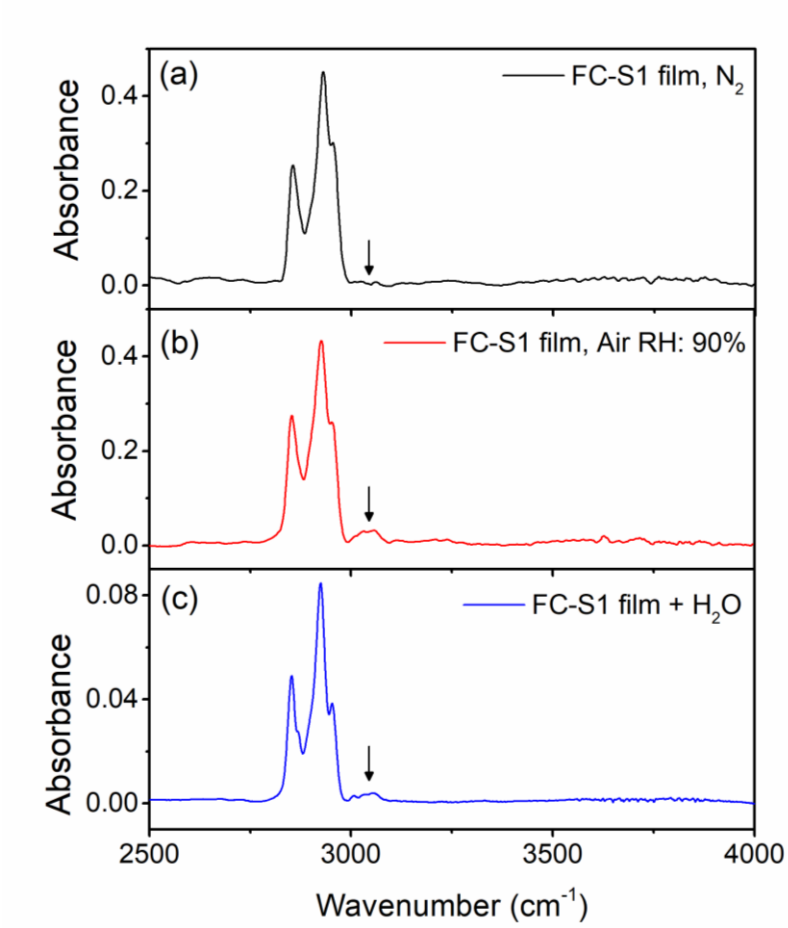

Fig. S3 FT-IR spectra FC-S1 films by drop casting FC-S1 chloroform solution in (a) N_2 glovebox and (b) air with 90% RH as well as (c) drop casting FC-S1 chloroform solution with small amount of water (20 μL water in 200 μL chloroform) in air with 70% RH. For the FC-S1 film by drop casting in air with 90% RH, the FTIR spectrum can show the H_2O peak in range of 3000–3100 cm^{-1} whereas such a H_2O peak does not exist in the FC-S1 film by drop casting in the N_2 glovebox.

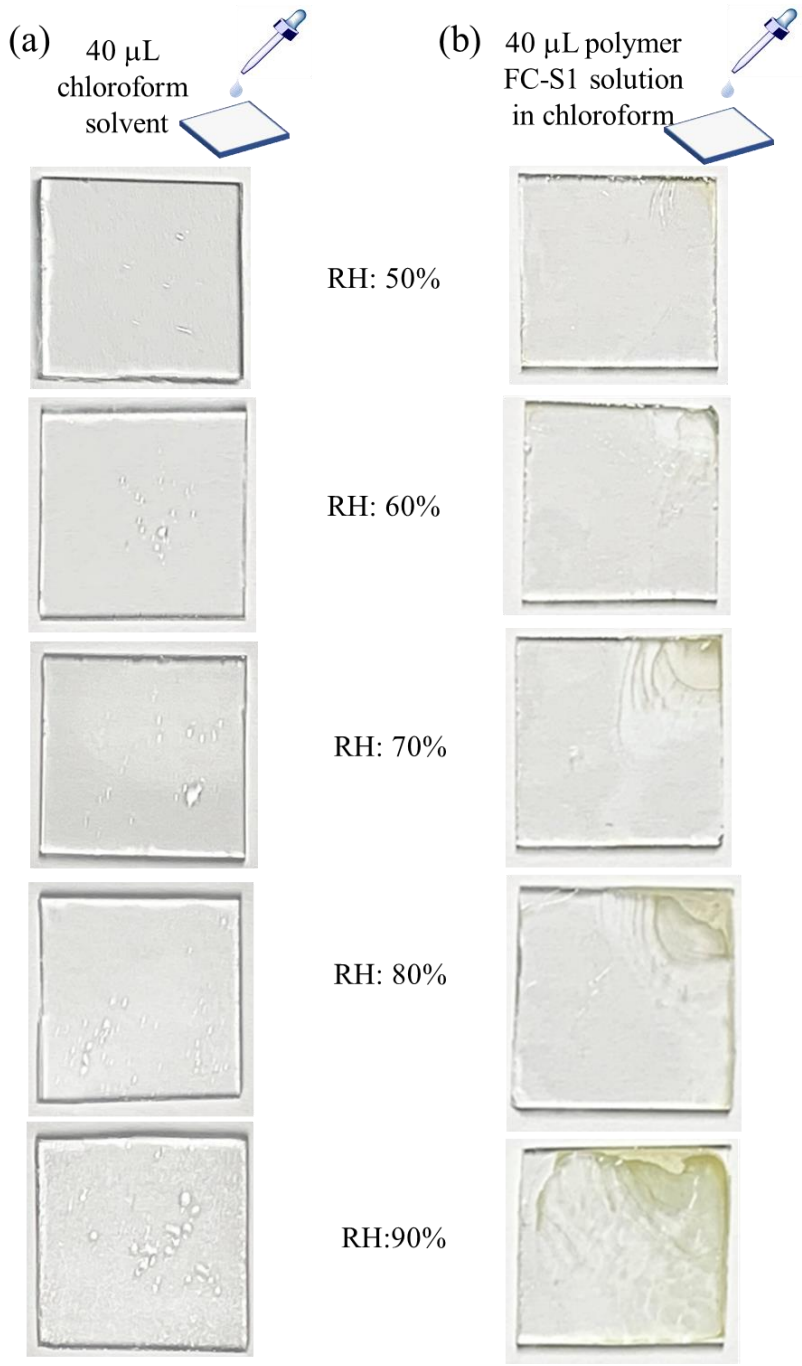

Fig. S4 Moisture condensations on the substrate after evaporations of (a) pure chloroform and (b) FC-S1 chloroform solution in air with different relative humidities (RH).

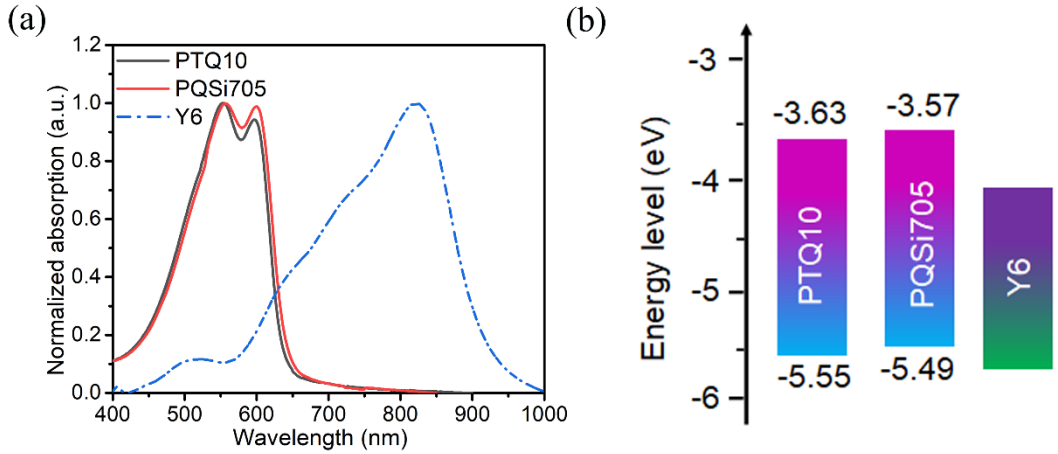

Fig. S5 (a) The film absorption spectra and (b) energy levels of PTQ10, PQSi705, and Y6.

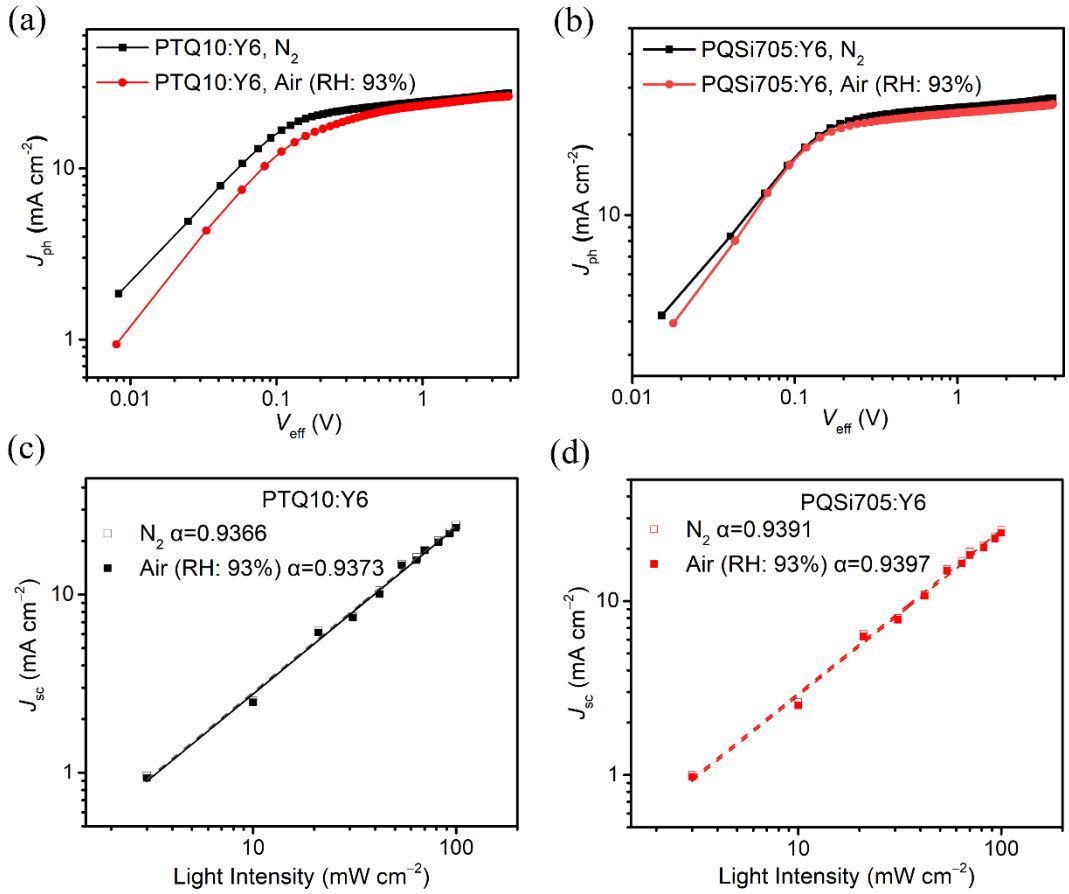

Fig. S6 J_{ph}-V_{eff} curves of (a) PTQ10:Y6 and (b) PQSi705:Y6 based devices processed in N_2 glovebox and air with 93% relative humidity. The dependency of J_{sc} on light intensity for (c) PTQ10:Y6 and (d) PQSi705:Y6 processed in N_2 glovebox and air with 93% relative humidity.

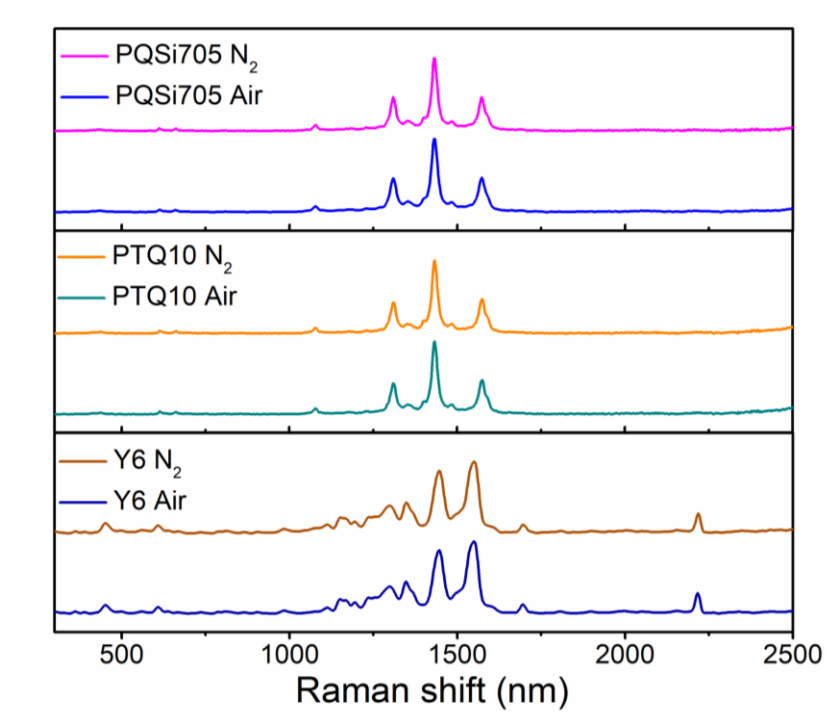

Fig. S7 The Raman spectra of the PQSi705, PTQ10 and Y6 neat films processed in N_2 glovebox and air with 93% RH, respectively.

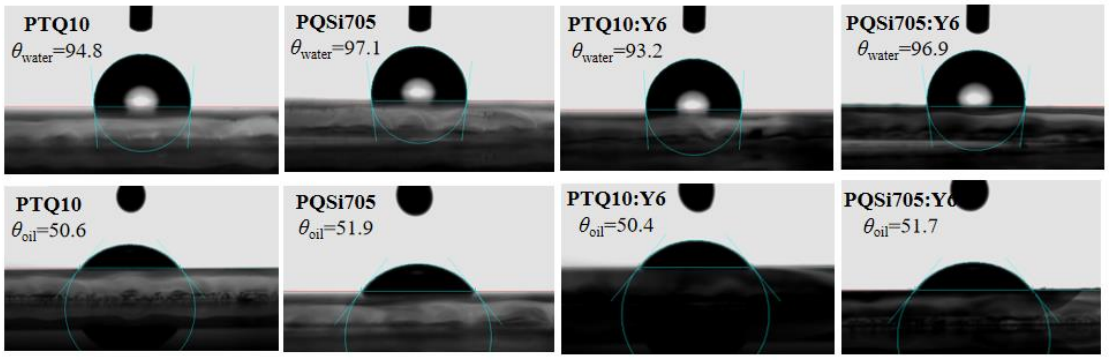

Fig. S8 The contact-angle test generated from oil and water droplets on the surface of polymer neat films and their blend films.

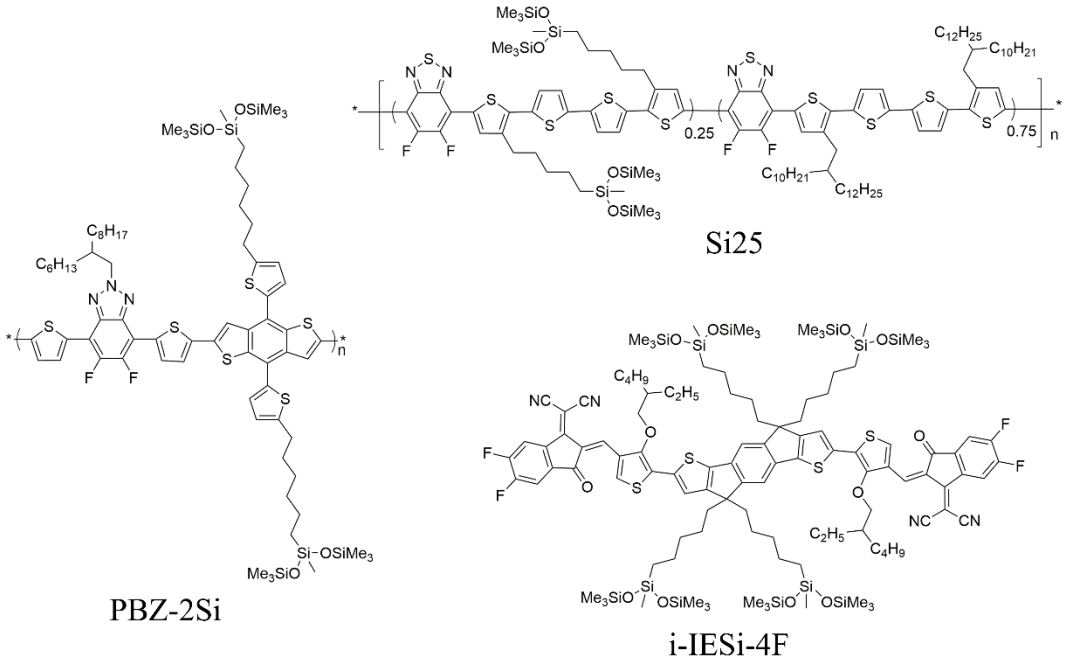

Fig. S9 Molecular structures of polymer donors PBZ-2Si and Si25 and non-fullerene acceptor i-IESi-4F.

Supplementary Tables

Table S1 The device performance of the air-processed organic solar cells reported in recent years

Entry	Active layer	Relative humidity [%]	V_{OC} [V]	J_{SC} [mA cm^{-2}]	FF [%]	PCE [%]	Ref.
1	P9:$PC_{71}BM$	--[a]	0.85	13.17	64	7.13	[7]
2	PCDTBT:GNF-EDNB:$PC_{71}BM$	--[a]	0.896	12.56	57.1	6.41	[8]
3	PDPPPTD:$PC_{71}BM$	--[a]	0.85	11.72	67	6.7	[9]
4	PFQ2T-BDT:$PC_{61}BM$	--[a]	0.87	8.70	55	4.2	[10]
5	PBDT-TSR:$PC_{71}BM$	--[a]	0.780	16.48	62.37	8.02	[11]
6	PDPPPTD:$PC_{61}BM$	--[a]	0.87	12.55	67.83	7.41	[12]
7	DRCN5T:$PC_{71}BM$	--[a]	0.92	15.48	59.30	8.5	[13]
8	PTB7-Th:tPDI-Hex	--[a]	0.94	11.6	43.7	4.8	[14]
9	PTB7-Th:PDI-DPP-PDI	--[a]	0.98	11.32	50.1	5.6	[15]
10	P-4FP:Y6	--[a]	0.80	20.73	72.67	12.05	[16]
11	PM6:BTP-eC9	25–35	0.836	26.26	76.4	16.77	[17]
12	PM6:ITIC-4F	30	0.823	18.06	71.6	10.77	[18]
13	PM6:Y7	30	0.857	22.95	69.7	13.44	[18]
14	PBDTTT-OFT:$PC_{71}BM$	35–45	0.481	2.1	47.4	0.49	[19]
15	PBDTTT-OFT:IEICO-4F	35–45	0.655	20.5	64.2	8.61	[19]
16	PM6:Y6	35–45	0.785	23.0	61.3	11.07	[19]
17	P(F-BiT)-COOBOCl (out):IT-4F	69	0.899	18.8	68.0	11.49	[20]
18	PBDB-T: N2200	80	0.86	10.97	64.2	6.06	[21]
19	PTB7-Th:PDI-V	90	0.74	15.3	64	7.3	[22]
20	**PQSi705:Y6**	**93**	**0.841**	**26.89**	**71.08**	**16.08**	**This work**
21	**PQSi705:*m*-TEH**	**90**	**0.887**	**26.72**	**76.55**	**18.00**	**This work**

[a] Relative humidity (RH) for the ambient condition is not indicated in the report

Table S2 Device performance parameters based on active layers of PM6:Y6, PM6:L8-BO and PM6:BTP-eC9 processed in a N_2 glovebox or air with 90% relative humidity

Active layer[a]	Condition	V_{OC} [V]	J_{SC} [mA cm^{-2}]	FF [%]	PCE[b] [%]
PM6:Y6	N_2	0.854	25.87	71.6	15.85
		(0.853 ± 0.006)	(25.05 ± 0.52)	(72.42 ± 0.85)	(15.36 ± 0.33)
	Air, RH:90%	0.831	25.24	66.63	13.98
		(0.833 ± 0.006)	(25.01 ± 0.34)	(65.56 ± 1.44)	(13.66 ± 0.44)
PM6:L8-BO	N_2	0.860	25.89	81.05	18.04
		(0.860 ± 0.001)	(25.60 ± 0.44)	(80.72 ± 0.57)	(17.77 ± 0.22)
	Air, RH:90%	0.849	25.30	75.14	16.18
		(0.838 ± 0.033)	(24.68 ± 0.65)	(72.18 ± 5.51)	(15.00 ± 1.76)
PM6:BTP-eC9	N_2	0.831	26.90	78.38	17.54
		(0.830 ± 0.003)	(26.90 ± 0.25)	(77.86 ± 0.76)	(17.40 ± 0.14)
	Air, RH:90%	\[c]	\[c]	\[c]	\[c]

[a] The D:A ratios of the active layers and the device preparations were according to literature reports.[23-25] [b] Statistical data in parentheses are average values with standard deviation from 10 independent devices. [c] The processing of PM6:BTP-eC9 in air with 90% RH leaded abnormal *J-V* curve and zero efficiency.

Table S3 J_{ph}, J_{sat}, dissociation efficiency (η_{diss}) and charge collection efficiency (η_{coll}) of PTQ10:Y6 and PQSi705:Y6 processed in a N_2 glovebox and air with 93% relative humidity

Active layer	Condition	J_{ph} [a] [mA/cm^2]	J_{ph} [b] [mA/cm^2]	J_{sat} [mA/cm^2]	η_{diss} [%]	η_{coll} [%]
PTQ10:Y6	N_2	24.36	20.80	25.47	95.56	81.66
	Air, RH 93%	22.93	16.38	24.27	94.46	67.49
PQSi705:Y6	N_2	25.31	22.77	26.08	97.01	87.29
	Air, RH 93%	25.43	22.37	26.04	97.65	85.91

[a] J_{ph} under short-circuit condition. [b] J_{ph} under maximal power output condition.

Table S4 Contact angles and surface energy parameters of the polymer neat films and blend films

surface	θ_{water} [deg]	θ_{oil} [deg][a]	γ^d [mJ/m^2] [b]	γ^p [mJ/m^2] [c]	γ[mJ/m^2]
PTQ10	94.8	50.6	34.12	0.99	35.11
PQSi705	97.1	51.9	34.82	0.09	34.93
PTQ10:Y6	93.2	50.4	33.77	1.60	35.38
PQSi705:Y6	96.9	51.7	34.74	0.17	34.92
Y6	82.3	35.6	39.71	4.22	43.92

[a] θ_{oil} represents the contact angle of diiodomethane. [b] γ^d represent the surface free energies generated from the dispersion forces and [c] γ^p represent the surface free energies generated from the polar forces.

Table S5 The device performance parameters of PTQ10:Y6 active layer after extremely harsh condition treatment

Condition	V_{OC} [V]	J_{SC} [mA cm^{-2}]	FF [%]	PCE[a] [%]
immersion in water	0.831	24.88	56.54	11.69
	(0.757 ± 0.07)	(24.49 ± 0.35)	(44.14 ± 9.09)	(8.33 ± 2.40)
exposing in boiling water vapor	0.824	25.26	57.85	12.00
	(0.706 ± 0.21)	(24.89 ± 0.69)	(47.38 ± 13.12)	(8.91 ± 4.19)

[a] Statistical data in parentheses are average values with standard deviation from 8 devices.

Table S6 Device performance parameters based on active layers of PQSi705:*m*-TEH, PBZ-2Si:i-IEICO-4F, Si25:Y6-BO, J52:i-IESi-4F and PBZ-2Si:i-IESi-4F processed in a N_2-filled glovebox and air with 90% relative humidity

Active layer	Condition	V_{OC} [V]	J_{SC} [mA cm^{-2}]	FF [%]	PCE[a] [%]
PQSi705:*m*-TEH	N_2	0.882 (0.881 ± 0.002)	27.10 (26.85 ± 0.20)	75.45 (74.78 ± 0.85)	18.02 (17.69 ± 0.16)
	Air, RH:90%	0.887 (0.887 ± 0.003)	26.72 (26.39 ± 0.36)	75.66 (76.16 ± 0.65)	18.00 (17.63 ± 0.18)
PBZ-2Si:i-IEICO-4F	N_2	0.889 (0.885 ± 0.005)	20.42 (20.06 ± 0.46)	71.60 (71.65 ± 0.82)	13.02 (12.73 ± 0.21)
	Air, RH:90%	0.892 (0.882 ± 0.006)	20.33 (20.01 ± 0.42)	71.73 (70.96 ± 0.64)	12.99 (12.54 ± 0.25)
Si25:Y6-BO	N_2	0.662 (0.653 ± 0.008)	26.34 (26.21 ± 0.88)	68.94 (68.22 ± 0.73)	12.03 (11.51 ± 0.37)
	Air, RH:90%	0.662 (0.657 ± 0.005)	26.50 (26.18 ± 0.86)	68.36 (67.78 ± 0.78)	12.01 (11.67 ± 0.38)
J52:i-IESi-4F	N_2	0.801 (0.803 ± 0.008)	22.47 (21.52 ± 0.54)	64.40 (64.15 ± 0.51)	11.60 (11.10 ± 0.35)
	Air, RH:90%	0.791 (0.799 ± 0.008)	22.50 (21.93 ± 0.30)	63.72 (63.52 ± 0.59)	11.35 (11.13 ± 0.31)
PBZ-2Si:i-IESi-4F	N_2	0.871 (0.869 ± 0.003)	23.25 (23.09 ± 0.49)	69.66 (68.94 ± 1.07)	14.11 (13.82 ± 0.17)
	Air, RH:90%	0.861 (0.864±0.005)	23.65 (23.32±0.40)	69.43 (68.79 ± 0.85)	14.14 (13.87 ± 0.18)

[a] Statistical data in parentheses are average values with standard deviation from 10 devices.

References

1 C. Sun, F. Pan, H. Bin, J. Zhang, L. Xue, B. Qiu, Z. Wei, Z.-G. Zhang and Y. Li, *Nat. Commun.*, 2018, **9**, 743.

2 D. Yuan, L. Zhang and J. Chen, *ChemSusChem*, 2022, **15**, e202200789.

3 H. Jiang, F. Pan, L. Zhang, X. Zhou, Z. Wang, Y. Nian, C. Liu, W. Tang, Q. Ma, Z. Ni, M. Chen, W. Ma, Y. Cao and J. Chen, *ACS Appl. Mater. Interfaces*, 2019, **11**, 29094-29104.

4 R. Qiu, Z. Wu, S. Li, H. Jiang, Q. Wang, Y. Chen, X. Liu, L. Zhang and J. Chen, *Sci. China Chem.*, 2021, **64**, 1208-1218.

5 X. Liu, L. Nian, K. Gao, L. Zhang, L. Qing, Z. Wang, L. Ying, Z. Xie, Y. Ma, Y. Cao, F. Liu and J. Chen, *J. Mater. Chem. A*, 2017, **5**, 17619-17631.

6 X. Liu, Z. Liu, M. Chen, Q. Wang, F. Pan, H. Liu, L. Zhang and J. Chen, *Macromol. Rapid Commun.*, 2022, **43**, 2200199.

7 A. Najari, S. Beaupré, N. Allard, M. Ouattara, J.-R. Pouliot, P. Charest, S. Besner, M. Simoneau and M. Leclerc, *Adv. Energy Mater.*, 2015, **5**, 1501213.

8 F. Bonaccorso, N. Balis, M. M. Stylianakis, M. Savarese, C. Adamo, M. Gemmi, V. Pellegrini, E. Stratakis and E. Kymakis, *Adv. Funct. Mater.*, 2015, **25**, 3870-3880.

9 M. Guérette, A. Najari, J. Maltais, J.-R. Pouliot, S. Dufresne, M. Simoneau, S. Besner, P. Charest and M. Leclerc, *Adv. Energy Mater.*, 2016, **6**, 1502094.

10 M. Prosa, M. Tessarolo, M. Bolognesi, O. Margeat, D. Gedefaw, M. Gaceur, C. Videlot-Ackermann, M. R. Andersson, M. Muccini, M. Seri and J. Ackermann, *ACS Appl. Mater. Interfaces*, 2016, **8**, 1635-1643.

11 L. Ye, Y. Xiong, H. Yao, A. Gadisa, H. Zhang, S. Li, M. Ghasemi, N. Balar, A. Hunt, B. T. O'Connor, J. Hou and H. Ade, *Chem. Mater.*, 2016, **28**, 7451-7458.

12 C. Wang, S. Ni, S. Braun, M. Fahlman and X. Liu, *J. Mater. Chem. C*, 2019, **7**, 879-886.

13 Y.-M. Sung, C.-S. Tsao, H.-K. Lin, H.-C. Cha and Y.-C. Huang, *Sol. Energy*, 2022, **231**, 536-545.

14 S. V. Dayneko, A. D. Hendsbee and G. C. Welch, *Chem. Commun.*, 2017, **53**, 1164-

1167.

15 S. M. McAfee, S. V. Dayneko, P. Josse, P. Blanchard, C. Cabanetos and G. C. Welch, *Chem. Mater.*, 2017, **29**, 1309-1314.

16 Z. Zheng, E. He, Y. Lu, Y. Yin, X. Pang, F. Guo, S. Gao, L. Zhao and Y. Zhang, *ACS Appl. Mater. Interfaces*, 2021, **13**, 15448-15458.

17 Y. Zhang, K. Liu, J. Huang, X. Xia, J. Cao, G. Zhao, P. W. K. Fong, Y. Zhu, F. Yan, Y. Yang, X. Lu and G. Li, *Nat. Commun.*, 2021, **12**, 4815.

18 T. Kumari, J. Oh, S. M. Lee, M. Jeong, J. Lee, B. Lee, S.-H. Kang and C. Yang, *Nano Energy*, 2021, **85**, 105982.

19 A. Maeda, R. Liu, K. Yu, S. Lee, K. Nakano, M. Takakuwa, S. Zhang, K. Tajima, K. Fukuda, S. Umezu and T. Someya, *J. Phys. Mater.*, 2021, **4**, 044016.

20 S. J. Jeon, Y. H. Kim, D. H. Hong, N. G. Yang, Y. W. Han and D. K. Moon, *Sol. RRL*, 2021, **5**, 2000608.

21 Y. Xu, J. Yuan, S. Zhou, M. Seifrid, L. Ying, B. Li, F. Huang, G. C. Bazan and W. Ma, *Adv. Funct. Mater.*, 2019, **29**, 1806747.

22 Y. Guo, Y. Li, O. Awartani, J. Zhao, H. Han, H. Ade, D. Zhao and H. Yan, *Adv. Mater.*, 2016, **28**, 8483-8489.

23 L. Zhu, M. Zhang, J. Xu, C. Li, J. Yan, G. Zhou, W. Zhong, T. Hao, J. Song, X. Xue, Z. Zhou, R. Zeng, H. Zhu, C.-C. Chen, R. C. I. MacKenzie, Y. Zou, J. Nelson, Y. Zhang, Y. Sun and F. Liu, *Nature Materials*, 2022, **21**, 656-663.

24 Y. Cui, H. Yao, J. Zhang, K. Xian, T. Zhang, L. Hong, Y. Wang, Y. Xu, K. Ma, C. An, C. He, Z. Wei, F. Gao and J. Hou, *Adv. Mater.*, 2020, **32**, 1908205.

25 J. Yuan, Y. Zhang, L. Zhou, G. Zhang, H.-L. Yip, T.-K. Lau, X. Lu, C. Zhu, Hongjian Peng, P. A. Johnson, M. Leclerc, Y. Cao, J. Ulanski, Y. Li and Y. Zou, *Joule*, 2019, **3**, 1-12.